

DEPARTMENT OF MATHEMATICAL SCIENCES
COLLEGE OF SCIENCES
OLD DOMINION UNIVERSITY
NORFOLK, VIRGINIA 23508

DAN / LANGLEY
P. 133

NAG-1-704

FILE

82557 - CR

**MATHEMATICAL MODELING OF A
Ti:SAPPHIRE SOLID-STATE LASER**

By

John J. Swetits, Principal Investigator

Final Report
For the period ending May 15, 1987

Prepared for the
National Aeronautics and Space Administration
Langley Research Center
Hampton, VA 23665

Under
Research Grant NAG-1-704
Dr. Charles E. Byvik
FED-Laser Technology and Applications Branch

(NASA-CR-181105) MATHEMATICAL MODELING OF A
Ti:SAPPHIRE SOLID-STATE LASER Final Report,
period ending 15 May 1987 (Old Dominion
Univ.) 33 p Avail: NTIS HC A03/MF A01

N87-27168

CSCL 20E G3/36

Unclas
0082557

May 1987

DEPARTMENT OF MATHEMATICAL SCIENCES
COLLEGE OF SCIENCES
OLD DOMINION UNIVERSITY
NORFOLK, VIRGINIA 23508

**MATHEMATICAL MODELING OF A
TI:SAPPHIRE SOLID-STATE LASER**

By

John J. Swetits, Principal Investigator

Final Report
For the period ending May 15, 1987

Prepared for the
National Aeronautics and Space Administration
Langley Research Center
Hampton, VA 23665

Under
Research Grant NAG-1-704
Dr. Charles E. Byvik
FED-Laser Technology and Applications Branch

Submitted by the
Old Dominion University Research Foundation
P.O. Box 6369
Norfolk, Virginia 23508



May 1987

ABSTRACT

The project initiated a study of a mathematical model of a tunable Ti:Sapphire solid-state laser. A general mathematical model was developed for the purpose of identifying design parameters which will optimize the system, and serve as a useful predictor of the system's behavior.

PRECEDING PAGE BLANK NOT FILMED

TABLE OF CONTENTS

	<u>Page</u>
ABSTRACT.....	iii
INTRODUCTION.....	1
THE RATE EQUATIONS.....	2
QUALITATIVE ANALYSIS OF THE EQUATIONS.....	8
NUMERICAL ANALYSIS.....	16
SUMMARY AND CONCLUSION.....	24
ADDENDUM.....	27
ACKNOWLEDGMENTS.....	27
REFERENCES.....	27

LIST OF TABLES

<u>Table</u>	<u>Page</u>
1 Numerical values of the parameters used in these calculations. Values come from measurements reported in References 5 and 6.....	17

LIST OF FIGURES

<u>Figure</u>	<u>Page</u>
1 Energy level diagram for the model four level laser. Only those non-radiative transition to or from the lasing levels are shown in this figure.....	3
2 Computed curves showing the evolution of the inverted population density and the photon density for an end-pumped laser. Both densities are normalized to the density of dopant ions in the laser heads.....	19
3 Curves showing the effect of increasing the intensity of the pump beam. The strength of the output pulse increases with pump intensity.....	21
4 Extreme values of pump energy computed using a backward difference algorithm on the CYBER CY 173.....	22
5 Stiffening of the equations with increasing pump energy displayed in terms of the number of derivative evaluations required in the Runge-Kutta-Fehlberg algorithm.....	23

TABLE OF CONTENTS - continued

LIST OF FIGURES - continued

<u>Figure</u>		<u>Page</u>
6	The effects of increasing the intensity of the injection signal is to initiate the laser pulse at earlier times and to narrow the pulse shape.....	25
7	Inversion and photon densities illustrating relaxation oscillations before stable solution is reached. Individual curves are combined together in a phase portrait.....	26

MATHEMATICAL MODELING OF A TI:SAPPHIRE SOLID-STATE LASER

By

John J. Swetits*

INTRODUCTION

Recently, several new experimental techniques involving the transient behavior of solid state lasers have been developed to control the frequency and shape of a laser beam (1-4). Among these is injection seeding, a technique which relies upon precise timing between the pumping beam, the injection beam and the onset of lasing action. Its effective use requires accurate understanding of the temporal development of the laser dynamical variables. It follows that there is a need to reexamine the transient behavior of the laser under the conditions which prevail in this situation. In order to study the use of injection seeding and other similar techniques, we have developed a model of the dynamical process in a four-level solid-state laser. The analysis was developed for the Titanium-doped Sapphire system, but it is of a general character, and can be applied broadly with minor modification to any system.

In solid-state lasers the optically active ions are fixed in place within a transparent host. In Ti:Sapphire, the Ti^{3+} ion substitutes for the Al^{3+} ion in Al_2O_3 to a concentration of about 1%. Because of a strong coupling between the active ion and the host lattice the absorption and emission lines are broadened and the material can lase at over a range of wavelengths. If left running freely, the laser will operate at a wavelength near to the peak of the emission cross-section. By introducing an injection signal the laser can be made to lase at a different wavelength. The solid-state laser material is formed into a cylindrical rod with its axis

*Professor, Department of Mathematical Sciences, Old Dominion University, Norfolk, Virginia 23508.

coincident with the optical axis of a Fabry-Perot cavity. This rod is presumed to be pumped axially by another laser at the pumping wavelength although this mode of pumping is not critical to the model. In addition, an injection signal, at the desired lasing wavelength, is injected axially into the material.

The model describes the time evolution of the occupancy of the electronic levels and of the lasing photon flux concentration within the cavity. Most of the parameters used in the model can be obtained by direct measurement; the effects of the few quantities which cannot be directly measured are studied parametrically. The main purpose of this effort is to understand the temporal characteristics of injection seeding on solid-state lasers and so the model avoids some complications of laser operation which are not essential to this objective. For example, it treats a single lasing wavelength with a narrow bandwidth. It also does not directly treat the spatial distribution of excitation in the rod, but considers the spatial average over the rod as a whole.

In the next section, the basic system of equations for the electron and photon populations are introduced and put into the form finally used. Following that, the quantitative properties of the solutions to this system is derived. The system is proven to be asymptotically stable and general bounds on the population inversion are obtained. After that a numerical analysis of the system is described and solutions obtained.

THE RATE EQUATIONS

The emission and absorption spectra of $\text{Ti}^{3+}:\text{Al}_2\text{O}_3$ (5-6) are the basis for an idealized four-level model of the lasing action of Titanium in Sapphire shown in Fig. 1.

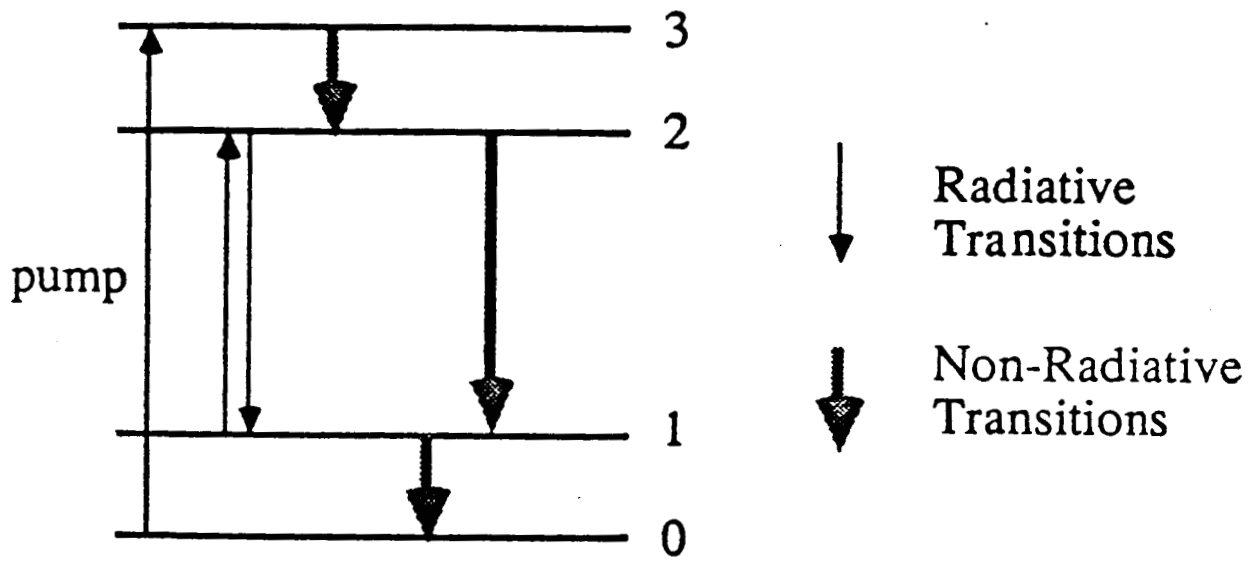


Figure 1. Energy level diagram for the model four level laser. Only those non-radiative transition to or from the lasing levels are shown in this figure.

The rate equations giving the time dependence of the population densities, $n_i(t)$, for each of the electronic levels for this system are given below.

$$\frac{dn_3}{dt} = W_{03} n_0 - \frac{n_3}{\tau_3} \quad (1)$$

$$\frac{dn_2}{dt} = \frac{n_3}{\tau_{32}} - \left(n_2 - \frac{g_1}{g_2} n_1 \right) \sigma \phi v - \frac{n_2}{\tau_2} \quad (2)$$

$$\frac{dn_1}{dt} = \frac{n_3}{\tau_{31}} + \frac{n_2}{\tau_{21}} - \left(n_2 - \frac{g_1}{g_2} n_1 \right) \sigma \phi v - \frac{n_1}{\tau_1} \quad (3)$$

In these equations τ_i is the lifetime for the i^{th} electronic level, while τ_{ij}^{-1} is the rate for the transition from level i to level j . These rates are related by reciprocal sum rule

$$\tau_i^{-1} = \sum_j \tau_{ij}^{-1} \quad .$$

$W_{03}(t)$ is the pumping rate giving the number of photons per second pumped to level 3 from the ground state. The degeneracy of the i^{th} electron level is g_i . The population densities, n_i , for each of the laser levels are constrained by the relation

$$n_{\text{TOTAL}} = n_0 + n_1 + n_2 + n_3, \quad (4)$$

where n_{TOTAL} is the dopant concentration. The photon concentration (number of photons per cm^3) within the lasing medium is represented by $\phi(\lambda)$, the emission cross-section by σ and the speed of light in the crystal by v . The rate of change of the photon concentration is given by the following expression:

$$\frac{d\phi}{dt} = (n_2 - \frac{g_1}{g_2} n_1) \sigma \phi v - \frac{\phi}{\tau_c} + S_p \quad (5)$$

Here τ_c is the cavity lifetime and it represents the loss of photons from all mechanisms in the cavity; S_p is the contribution to the photon flux in the laser beam coming from the spontaneous emission of excited atoms. It is expressed as a fraction S_{po} of the total fluorescence decay rate, τ_{fl} . S_{po} depends both on the geometry of the laser cavity and on the fluorescence spectrum of the lasing ion.

We can simplify these equations somewhat without losing generality. First, we assume that the non-radiative decay from the pumped level to the upper lasing level is fast, $\tau_3 \gg$ all other time scales. Then, integrating the rate equation for n_3 with this assumption, we obtain

$$n_3(t) \approx W_{03}(t)n_0(t)\tau_3$$

so that n_3 can be replaced by this expression in the subsequent equations. This condition is equivalent to assuming that $dn_3/dt=0$. Furthermore, we assume that the dominant decay path from level 3 is the non-radiative decay to level 2, that is $\tau_{32} \ll \tau_{31}$ and τ_{30} , so that $\tau_3 \approx \tau_{32}$. In this case the pumped photons are transferred to the upper laser level at a rate

$$(n_3/\tau_{32}) = W_{03}n_0(\tau_3/\tau_{32}) = W_p n_0,$$

and $n_3/\tau_3 = 0$. Furthermore, if $n_3 \ll n_i$ for $i = 0, 1, \text{ or } 2$, so that not many electrons stay in their pumped level

$$n_{\text{TOTAL}} = n_0 + n_1 + n_2 + n_3 \approx n_0 + n_1 + n_2.$$

Now the decay from level 2 has both radiative and non-radiative contributions which are related by

$$\tau_2^{-1} = \tau_{f1}^{-1} + \tau_{NR}^{-1} \quad (6)$$

With these assumptions the rate equations for the electron concentrations become:

$$\frac{dn_2}{dt} = W_p n_0 - (n_2 - \frac{g_1}{g_2} n_1) \sigma \phi v - \frac{n_2}{\tau_2} \quad (7)$$

$$\frac{dn_1}{dt} = \frac{n_2}{\tau_{f1}} + (n_2 - \frac{g_1}{g_2} n_1) \sigma \phi v - \frac{n_1}{\tau_1} \quad (8)$$

$$n_{\text{TOTAL}} = n_0 + n_1 + n_2 \quad (9)$$

Equations (5), (7), (8) and (9) form the basis of this model. We reorganize them slightly. First, we introduce new variables replacing the laser level populations, n_1 and n_2 , with the population inversion $n = n_2 - (g_2/g_1)n_1$, and

n_1 , the lower laser level population. Next we scale these new variables and the photon concentration to the total concentration of ions, n_{TOTAL}

$$\begin{aligned} x &= n/n_{TOTAL}, \\ y &= n_1/n_{TOTAL}, \text{ and} \\ z &= \phi/n_{TOTAL} \quad . \end{aligned}$$

Finally, we scale the time variable to the time interval, τ_N , taken here to be one nanosecond. With these changes the laser dynamic equations assume the form

$$\dot{\mathbf{v}} = \mathbf{C}\mathbf{v} + \alpha \begin{pmatrix} -\gamma \\ 1 \\ 1 \end{pmatrix} (xz) + \begin{pmatrix} W_p \\ 0 \\ 0 \end{pmatrix} (1-x-\gamma y) + I(t) \quad .$$

In this expression, \mathbf{v} is a vector with components equal to the three normalized concentrations (x,y,z) . The matrix \mathbf{C} representing the linear part of the differential equation has components given below.

$$\begin{aligned} c_{11} &= - \left(\frac{1}{\tau_2} + \frac{\gamma-1}{\tau_{fl}} \right) & c_{12} &= (1-\gamma) \left[\frac{1}{\tau_2} + \frac{\gamma-1}{\tau_{fl}} - \frac{1}{\tau_1} \right] & c_{13} &= 0 \\ c_{21} &= \frac{1}{\tau_{fl}} & c_{22} &= \frac{\gamma-1}{\tau_{fl}} - \frac{1}{\tau_1} & c_{23} &= 0 \\ c_{31} &= \frac{S_{p0}}{\tau_{fl}} & c_{32} &= (\gamma-1)c_{31} & c_{33} &= - \frac{1}{\tau_c} \end{aligned}$$

The second term has the non-linearity of the system as the product of the population inversion and photon concentration. The strength of this non-linearity is given by the parameter.

$$\alpha = \sigma v n_{\text{TOTAL}} \tau_N \cdot$$

Physically this quantity represents the number of ions seen by a photon in time τ_N . The parameter $\gamma = 1 + g_2/g_1$ is related to the multiplicities of the electronic states g_2 ; for Titanium:Sapphire $\gamma = 5/3$. In this last form of the equations we have introduced the possibility of stimulating emission with an injection beam $I(t)$. The notation $(1-x-\gamma y)_+$ means

$$(1-x-\gamma y)_+ = \begin{cases} 1-x-\gamma y & \text{if } 1-x-\gamma y > 0 \\ 0 & \text{if } 1-x-\gamma y < 0 \end{cases} \cdot$$

QUALITATIVE ANALYSIS OF THE EQUATIONS

The purpose of this section is to establish a number of qualitative properties of the solutions to the system [10]. We assume the physical parameters satisfy

$$0 < \tau_1 \ll \tau_1 < \tau_{fl}$$

$$0 < S_{po}$$

$$0 < \tau_c \cdot$$

Theorem: If $W_p(t)$, $I(t)$ are positive, continuous and integrable on

$[0, +\infty)$ and if $x(0) > 0$, $y(0) > 0$, $z(0) > 0$ then

- (i) $x(t) > 0$, $y(t) > 0$, $z(t) > 0$ for all t ;
- (ii) $x(t)$, $y(t)$, $z(t)$ are integrable on $(0, +\infty)$;
- (iii) The system (10) is asymptotically stable;
- (iv) If $x(0) + \gamma y(0) < 1$, then $x(t) + \gamma y(t) < 1$ for all t ; and
- (v) If $x(0) + \gamma y(0) > 1$, then there exists T

such that $x(t) + \gamma y(t) < 1$ for all $t > T$.

Proof: We establish the parts of the theorem in the order (iv), (v), (i), (ii), (iii).

- (vi) Since $x(0) + \gamma y(0) < 1$, then, by continuity, $x(t) + \gamma y(t) < 1$ for t close to 0. Suppose $x(T) + \gamma y(T) = 1$ and $x(t) + \gamma y(t) < 1$ for $t < T$. Then, at $t = T$,

$$\frac{d}{dt} (x + \gamma y) = (c_{11} + \gamma c_{21})x + (c_{12} + \gamma c_{22})y.$$

Since $c_{11} + \gamma c_{21} < 0$ and $c_{12} + \gamma c_{22} < 0$, then, if $x(T) > 0$ and $y(T) > 0$ and not both are zero, we would have

$$\frac{d}{dt} (x + \gamma y) < 0$$

at $t = T$ which would contradict $x(t) + \gamma y(t) < 1$ for $t < T$. Since $x(T) + \gamma y(T) = 1$, not both $x(T)$ and $\gamma(T)$ are zero.

Suppose $y(T) < 0$. Since $y(0) > 0$, there exists $T_1 < T$ such that $y(T_1) = 0$ and $y(t) > 0$ for $0 < t < T_1$. Then, at $t = T_1$,

$$\frac{dy}{dt} = c_{21} x + \alpha x z = (c_{21} + \alpha z)x.$$

Suppose $x(T_1) < 0$ and $c_{21} + \alpha z(T_1) > 0$. Then there exists $T_2 < T_1$ such that $x(T_2) = 0$ and $x(t) > 0$ for $0 < t < T_2$. Then at $t = T_2$

$$\begin{aligned} \frac{dx}{dt} &= c_{12}y(T_2) + W_p(T_2) (1 - \gamma y(T_2)) \\ &> 0 \end{aligned}$$

since $c_{12} > 0$, $y(T_2) > 0$, $W_p(T_2) > 0$ and $1 - \gamma y(t_2) > 0$.

Hence x increases to the right of T_2 . It follows that x cannot be negative for $0 < t < T_1$. So $x(T_1) > 0$.

Now suppose $c_{21} + \alpha z(T_1) < 0$. Since $c_{21} > 0$, $\alpha > 0$, then $z(T_1) < 0$. So there exists $T_3 < T_1$ such that $z(T_3) = 0$ and $z(t) > 0$ for $0 < t < T_3$. Then, at $t = T_3$,

$$\frac{dz}{dt} = c_{31} x + c_{32} = y + I(T_3) > 0$$

since $I(T_3) > 0$ and all other quantities are non-negative. Hence z increases to the right of T_3 . So it follows that $z(T_1) > 0$.

Now suppose $x(T_1) = 0$ so that

$$\frac{dy}{dt} = 0 \text{ at } t = T_1. \text{ Then, at } t = T_1,$$

$$\frac{dx}{dt} = W_p(T_1) > 0.$$

Additionally, at $t = T_1$,

$$\begin{aligned} \frac{d^2 y}{dt^2} &= c_{21} \frac{dx}{dt} + c_{22} \frac{dy}{dt} + \alpha \left(z \frac{dx}{dt} + x \frac{dz}{dt} \right) \\ &= c_{21} W_p(T_1) + \alpha z(T_1) W_p(T_1) > 0 \end{aligned}$$

since $c_{21} > 0$, $W_p(T_1) > 0$, $\alpha > 0$ and $z(T_1) > 0$. Thus y increases to the right of T_1 . It now follows that $y(T) > 0$.

Now suppose $x(T) < 0$. Choose $T_1 < T$ such that $x(T_1) = 0$ and $x(t) > 0$ for $0 > t > T_1$. Then, at $t = T_1$,

$$\frac{dx}{dt} = c_{21} y + W_p(T_1)(1 - \gamma y) > 0$$

since $y(T_1) > 0$, $c_{21} > 0$, $W_p(T_1) > 0$ and $1 - \gamma y(T_1) > 0$. Hence x increases to the right of T_1 . It follows that $x(T) > 0$.

Since at least one of $x(T)$, $y(T)$ is strictly positive, then at $t = T$,
 $\frac{d}{dt}(x + \gamma y) < 0$.

So $x + \gamma y$ is decreasing at $t = T$ which contradicts $x + \gamma y < 1$ for $t < T$. Thus $x(t) + \gamma y(t) < 1$ for all t .

(v) The proof of (iv) shows that if $x(0) + \gamma y(0) = 1$, then $x(t) + \gamma y(t) < 1$ for all $t > 0$.

Suppose $x(0) + \gamma y(0) > 1$. Then, for t close to 0,

$$\begin{aligned} \frac{d}{dt}(x + \gamma y) &= (c_{11} + \gamma c_{21})x + (c_{12} + \gamma c_{22})y \\ &< 0 \end{aligned}$$

by an argument similar to that given in (i). Thus $x + \gamma y$ is decreasing for t close to 0.

Suppose there exists $\lambda > 1$ such that $x + \gamma y > \lambda > 1$ for all t . Then

$$\begin{aligned} \frac{d}{dt}(x+\gamma y) &= (c_{11}+\gamma c_{21})(x+\gamma y) \\ &\quad + (c_{12}+\gamma c_{22}-\gamma(c_{11}+\gamma c_{21}))y \\ &< (c_{11}+\gamma c_{21})\lambda \end{aligned}$$

since $c_{12}+\gamma c_{22}-\gamma(c_{11}+\gamma c_{21}) < 0$ and $c_{11}+\gamma c_{21} < 0$. But then

$$x(t)+\gamma y(t)-(x(0)+\gamma y(0)) < (c_{11}+\gamma c_{21})\lambda t.$$

It follows that

$$\lim_{t \rightarrow \infty} (x(t)+\gamma y(t)) = -\infty$$

which contradicts $x+\gamma y > \lambda > 1$ for all t .

Thus there exists T such that $x(T)+\gamma y(T)=1$ and $x(t)+\gamma y(t) < 1$ for t close to T . The analysis in (i) now applies to show that $x(t)+\gamma y(t) < 1$ for all $t > T$.

- (i) The arguments in (iv) show that x, y , are non-negative on an interval where $x+\gamma y < 1$. Hence, if $x(0)+\gamma y(0) < 1$, then x, y , are non-negative for all t . Suppose there exists T such that $z(T) < 0$. Choose $T_1 < T$ such that $z(T_1)=0$. Then, at $t=T_1$,

$$\frac{dz}{dt} = c_{31}x+c_{32}y+I(T_1) > 0$$

since $c_{31} > 0, c_{32} > 0, x > 0, y > 0$ and $I(T_1) > 0$.

Hence z increases to the right of T_1 contradicting $z(T) < 0$. Thus, $z(t) > 0$ for all t .

To complete the picture, suppose $x(0)+\gamma y(0) > 1$. Choose T such that

$x(T) + \gamma y(T) = 1$ and $x(t) + \gamma y(t) > 1$ for $0 < t < T$. Then suppose $x(T_1) = 0$, $T_1 < T$, and $x(t) > 0$ for $0 < t < T_1$. Then at $t = T_1$,

$$\frac{dx}{dt} = c_{12}y.$$

Since $c_{12} > 0$ and $y(T_1) > 0$, x increases to the right of T_1 . Hence $x > 0$ for all t .

Now suppose $y(T_2) = 0$, $T_2 < T$ and $y(t) > 0$ for $0 < t < T_2$. At $t = T_2$,

$$\frac{dy}{dt} = c_{21}x + \alpha xz \quad .$$

Again $c_{21} > 0$, $x > 0$ and $z > 0$. So y increases to the right of T_2 . Hence $y > 0$ for all t .

(ii) Fix T so that $x(t) + \gamma y(t) < 1$ for $t > T$. Then

$$\begin{aligned} \frac{d}{dt}(x + \gamma y) &= (c_{11} + \gamma c_{21})(x + \gamma y) \\ &+ \\ &\quad (c_{12} + \gamma c_{22} - \gamma(c_{11} + \gamma c_{21}))y \\ &+ \\ &\quad W_p(1 - x - \gamma y) \\ &< (c_{11} + \gamma c_{21})(x + \gamma y) \\ &+ \\ &\quad W_p(1 - x - \gamma y) \end{aligned}$$

since $c_{12} + \gamma c_{22} - \gamma(c_{11} + \gamma c_{21}) < 0$ and $y > 0$.

Hence, letting

$$E(t) = \exp\left(\int_T^t (w_p - c_{11} - \gamma c_{21}) dr\right),$$

we have

$$\frac{d}{dt} (E(t) (x + \gamma y)) \leq E(t) w_p.$$

Thus,

$$E(t) (x + \gamma y) - (x(T) + \gamma y(T)) \leq \int_T^t E(u) w_p(u) du.$$

It follows that

$$\begin{aligned} 0 < x + \gamma y &\leq (E(t))^{-1} \left[\int_T^t E(u) w_p(u) du + x(T) + \gamma y(T) \right]. \\ &= \int_T^t (E(t) - E(u))^{-1} w_p(u) du + (E(t))^{-1} (x(T) + \gamma y(T)). \\ &\equiv R(t, T) \end{aligned}$$

Hence

$$0 < \int_T^S (x(t) + \gamma y(t)) dt \leq \int_T^S R(t, T) dt.$$

Note that, since $w_p > 0$,

$$\exp\left(-\int_u^t w_p(r) dr\right) \leq 1.$$

Thus

$$0 < \int_T^S (x(t) + \gamma y(t)) dt$$

$$\begin{aligned}
& \int_T^S W_p(u) \int_u^S \exp((c_{11} + \gamma c_{21})(t-u)) dt du \\
& \quad + \\
& \int_T^S \exp((c_{11} + \gamma c_{21})(t-T)) (x(T) + \gamma y(T)) dt \\
& = \int_T^S W_p(u) \left[\frac{\exp((c_{11} + \gamma c_{21})(s-u)) - 1}{c_{11} + \gamma c_{21}} \right] du \\
& \quad (x(T) + \gamma y(T)) \left[\frac{\exp((c_{11} + \gamma c_{21})(s-T)) - 1}{c_{11} + \gamma c_{21}} \right]
\end{aligned}$$

Since $c_{11} + \gamma c_{21} < 0$ and W_p is integrable on $[0, +\infty]$, it follows that $x + \gamma y$ is integrable on $[0, +\infty]$. Consequently both x and y are integrable since each is non-negative.

To see that z is integrable, note that

$$\begin{aligned}
& z(t) - \exp\left(\int_T^t (c_{33} + \alpha x) dr\right) z(T) \\
& = \exp\left(\int_T^t (c_{33} + \alpha x) dr\right) \int_T^t \exp\left(-\int_T^u (c_{33} + \alpha x) dr\right) (c_{31}x + c_{32}y + I) du
\end{aligned}$$

Using the fact that x, y, I are non-negative and integrable, an argument similar to the one above shows that z is integrable.

- (iii) Let X_0, Y_0, Z_0 solve the system (10). Let $x = X + X_0$, $y = Y + y_0$, $z = Z + z_0$. Assuming $x_0(0) + \gamma y_0(0) < 1$ and $x(0) + \gamma y(0) < 1$, we obtain the system

$$\frac{dX}{dt} = (c_{11} - \alpha \gamma z_0 - W_p) \underline{X} + (c_{12} - \gamma W_p) \underline{Y} - \alpha \gamma x_0 \underline{Z} - \alpha \gamma \underline{XZ}$$

$$\frac{dY}{dt} = (c_{21} + \alpha Z_0) \underline{X} + c_{22} \alpha x Z_0 + \alpha \underline{XZ}$$

$$\frac{dZ}{dt} = (c_{31} + \alpha Z_0) \underline{X} + c_{32} \underline{Y} + (c_{33} + \alpha x_0) \underline{Z} + \alpha \underline{XZ}$$

with $\underline{X}=\underline{Y}=\underline{Z}$ as a solution.

The linear system

$$\frac{dX}{dt} = c_{11} \underline{X} + c_{12} \underline{Y}$$

$$\frac{dY}{dt} = c_{21} \underline{Y} + c_{22} \underline{Y}$$

$$\frac{dZ}{dt} = c_{31} \underline{X} + c_{32} \underline{Y} + c_{33} \underline{Z}$$

is asymptotically stable since all eigenvalues of the coefficient matrix have negative real parts.

Since x_0, y_0, z_0, W_p are non-negative and integrable, it follows from Theorem 4.4 of [7] that $\underline{X}=\underline{Y}=\underline{Z}$ is an asymptotically stable solution of the non-linear system.

NUMERICAL ANALYSIS

In this section, we discuss the numerical solution to equations (5), (7), (8) and (9) subject to the quiescent initial conditions.

The equations were solved numerically on a DEC VAX 11/750 using a Runge-Kutta-Fehlberg (RKF) algorithm [8] and also on a CYBER CY173 using a backward difference method [9]. The time interval over which the solutions were computed was from 0 to 200 ns. Material parameters for Ti:Sapphire used in the examples are given in Table 1. We were interested in the qualitative behavior of the numerical solutions for various pumping rates

Table 1. Numerical values of the parameters used in these calculations. Values come from measurements reported in Refs. 5 and 6.

PARAMETERS

G2=2

G1=3

SIGMA=3.0E-19 cm²

INDEX OF REFRACTION=1.76

NTOTAL=1.0E18

TAUFL=3800ns

TAU1=1.0ns

TAUC=16.5ns

TAU2=3000ns

and injection strengths as well as the efficiency of the numerical procedures.

In the examples described here the pump and injection signals were both assumed to be Gaussian beams given by

$$W_p(t) = W f(t, t_p, \tau_p) \text{ and}$$

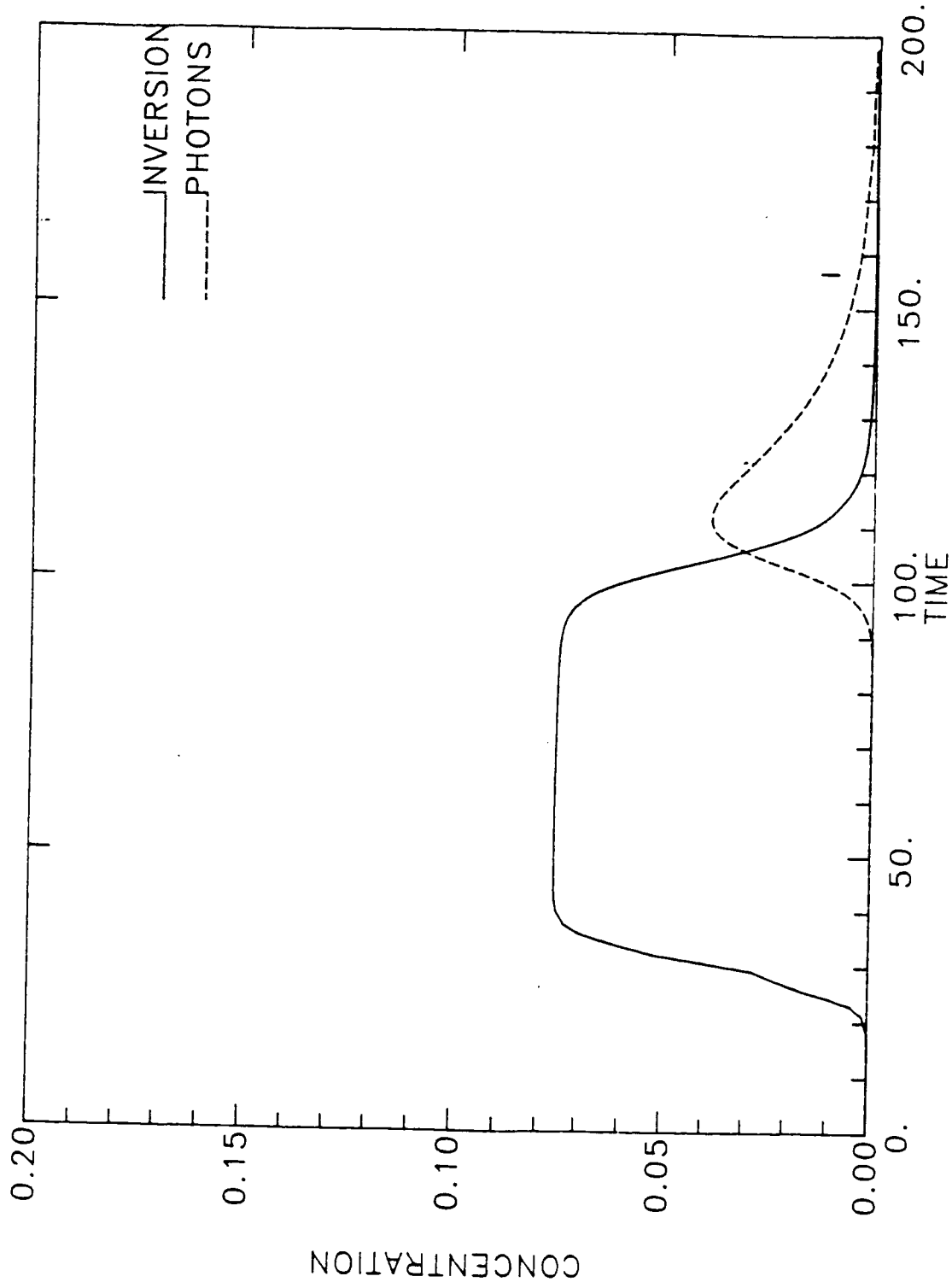
$$I(t) = I f(t, t_1, \tau_2) \text{ where}$$

$$f(t, t_0, \tau) = 2(\ln 2 / \pi)^{1/2} \exp(-\ln 2 ((t - t_0) / .5 * \tau)^2)$$

with $t_p = 30$ ns, $\tau_p = 10$ ns, $t_1 = 60$ ns, and $t_2 = 20$ ns. The values of W and I were varied. Increased values of W and I correspond to increases in the energies delivered by the pump and injection sources, respectively.

For relatively low values of W , the RKF algorithm was used to compute the solutions. All of the computations were done in double precision. In the examples, an error tolerance of 10^{-8} was used, but the qualitative behavior of the solutions was preserved for tolerances as large as 10^{-5} . Figure 2 shows a typical result of the computation.

The normalized population inversion and photon density are plotted as a function of time for a system in which the pumping rate W has the value $.01 \text{ ns}^{-1}$ and I has the value 0, i.e., no injection signal is present. Initially, the number of ions in the upper energy levels and the photon density in the medium is zero. At $t=0$, the pump is turned on and population inversion increases, following the leading edge of the pump pulse, until it has absorbed the photons in the pump beam and it levels off. During this



RATE EQUATION MODEL

Figure 2. Computed curves showing the evolution of the inverted population density and the photon density for an end-pumped laser. Both densities are normalized to the density of dopant ions in the laser head.

time the photon density has been increasing steadily (but not visibly on the graph). The dynamics up to this point are dominated by the linear part of the rate equations. The photon density increases until the non-linear term ($n \cdot \phi$) becomes comparable to the linear terms and it begins to dominate the dynamics. When this occurs there is a rapid increase in the photon density accompanied by a corresponding decrease in the population density. This latter exchange of photons for excited states by stimulated emission forms the shape of the laser pulse.

We varied the pumping rate W from $.01 \text{ ns}^{-1}$ to 1.0 ns^{-1} by orders of magnitude. It is evident from Fig. 3 that the larger the pumping rate, the earlier stimulated emission will occur and the stronger it will be. The RKF algorithm was found to perform very efficiently in the case where $W = .01 \text{ ns}^{-1}$ requiring only 822 evaluations of the derivatives. However, as the pump rate was increased, the number of derivative evaluations became much larger, with 1944 and 6612 evaluations needed when $W = .1 \text{ ns}^{-1}$ and $W = 1.0 \text{ ns}^{-1}$, respectively. The growth of the number of derivative evaluations with pump rate is shown in Figure 5.

For large values of W , the RKF algorithm failed to compute the solutions over the entire time interval in a reasonable number of iterations. W was set to 500 ns^{-1} and the RKF procedure required in excess of 67,000 derivative evaluations to compute the solutions from 0 to 44 ns. Using a backward difference method, the solutions, shown in Fig. 4, were found over the entire time interval 0 to 200 ns but 17,000 evaluations of the derivatives and 3700 evaluations of the Jacobean matrix were necessary. When the pump rates are high, the system of differential equations becomes stiff, resulting in considerable effort necessary to compute the solutions.

In order to examine the effect of the injection beam on the onset of

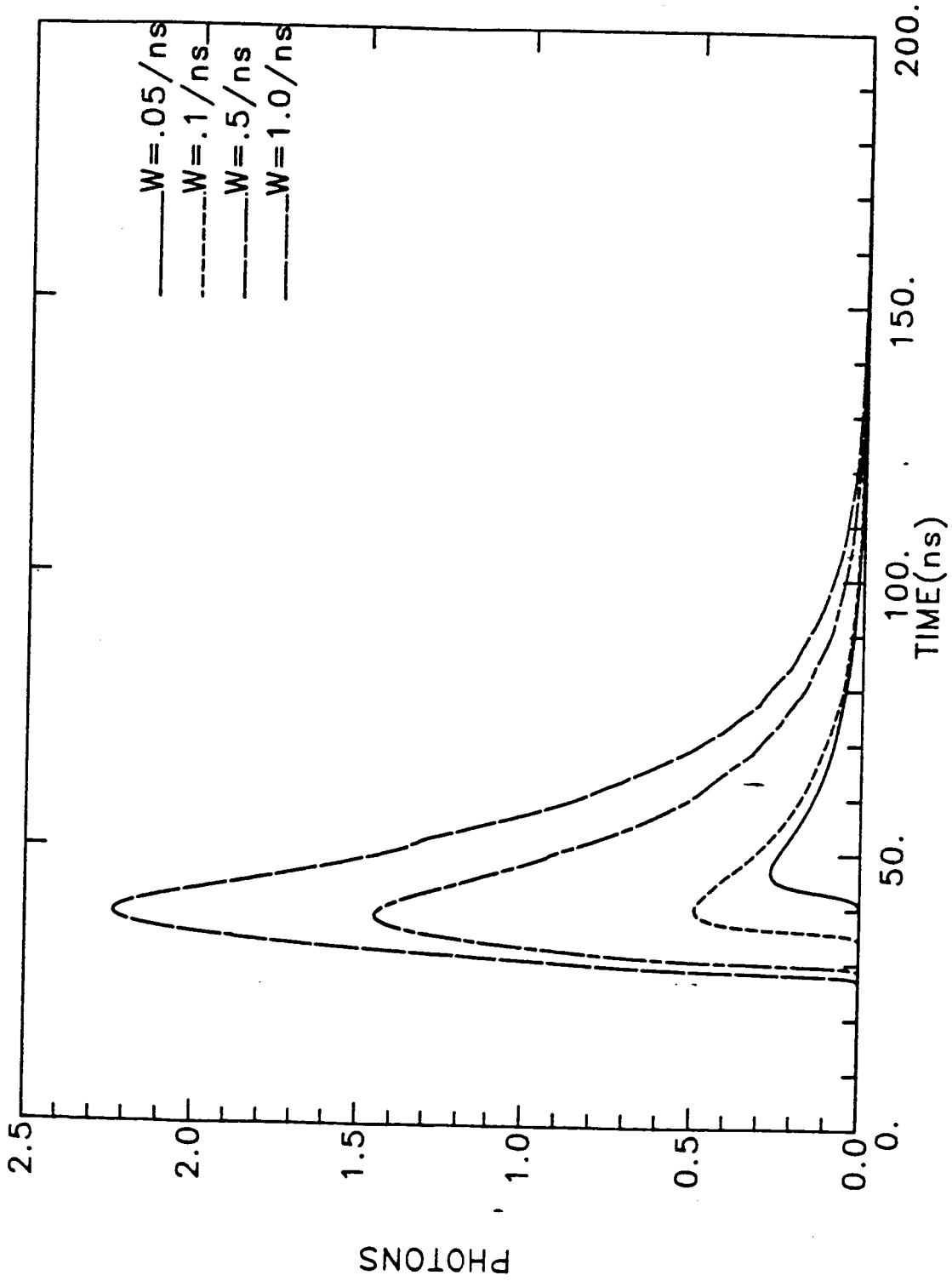


Figure 3. Curves showing the effect of increasing the intensity of the pump beam. The strength of the output pulse ion increases with pump intensity.

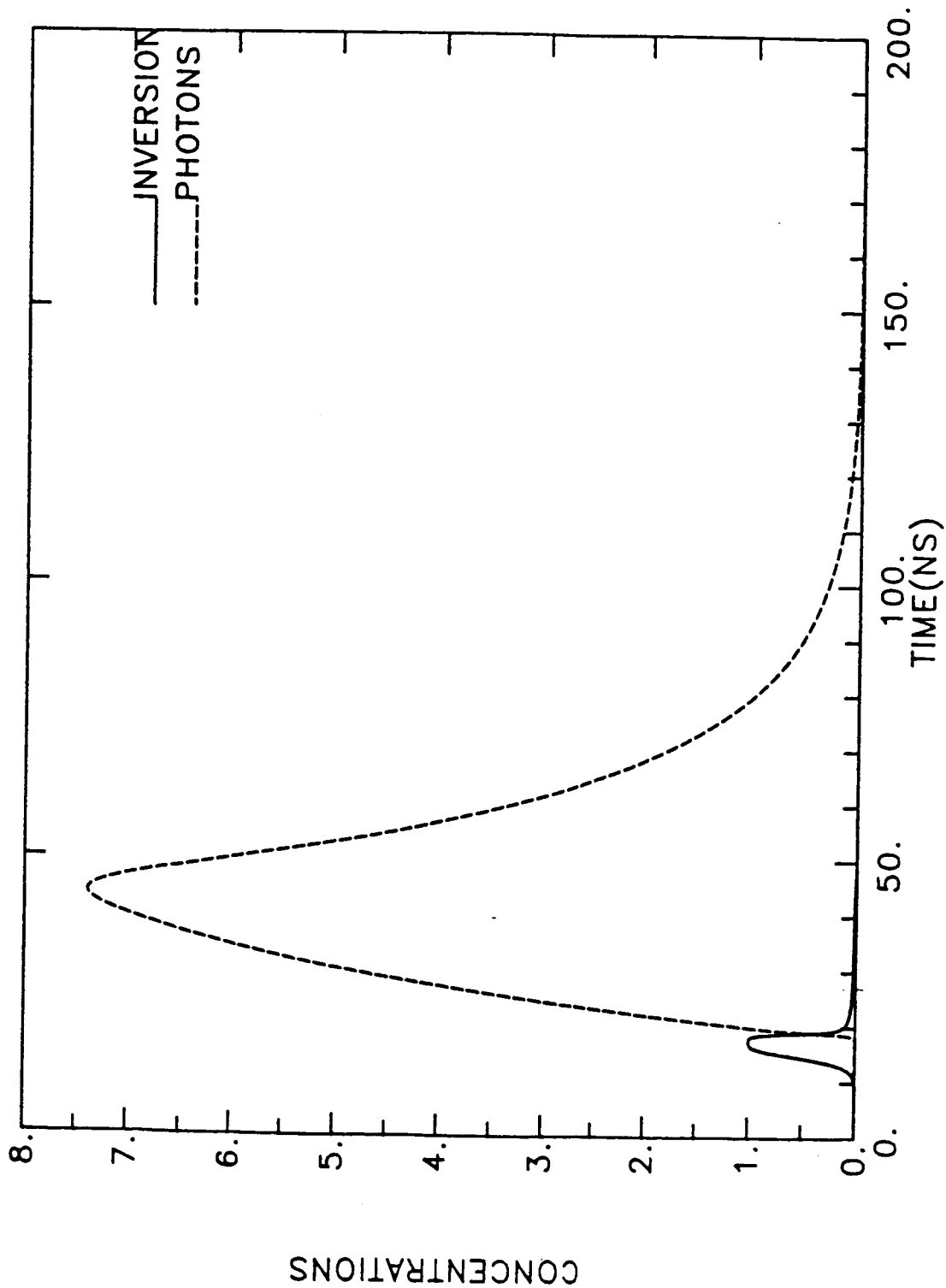


Figure 4. Extreme values of pump energy computed using a backward difference algorithm on the CYBER CY173.

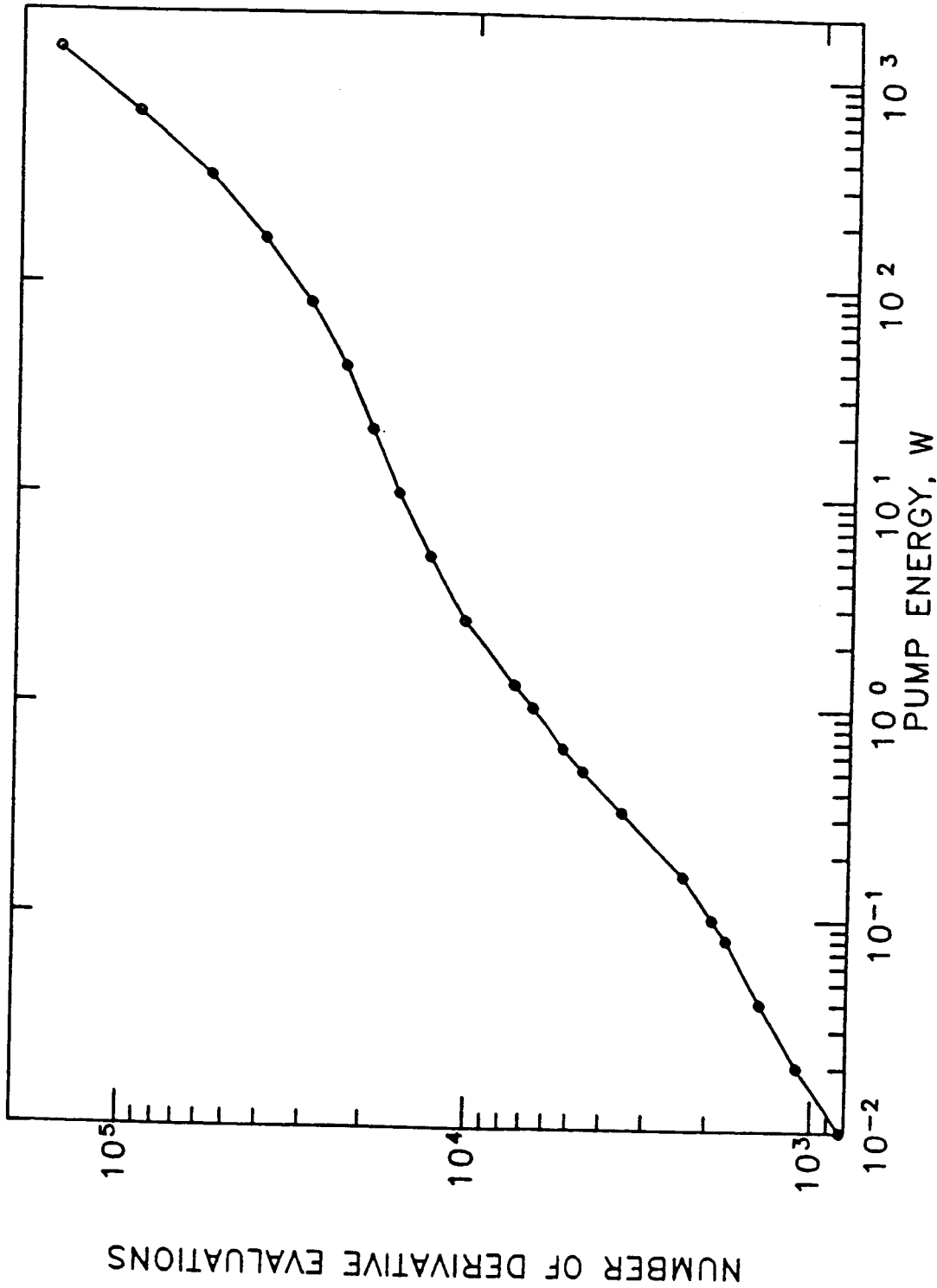


Figure 5. Stiffening of the equations with increasing pump energy displayed in terms of the number of derivative evaluations required in the Runge-Kutta-Fehlberg algorithm.

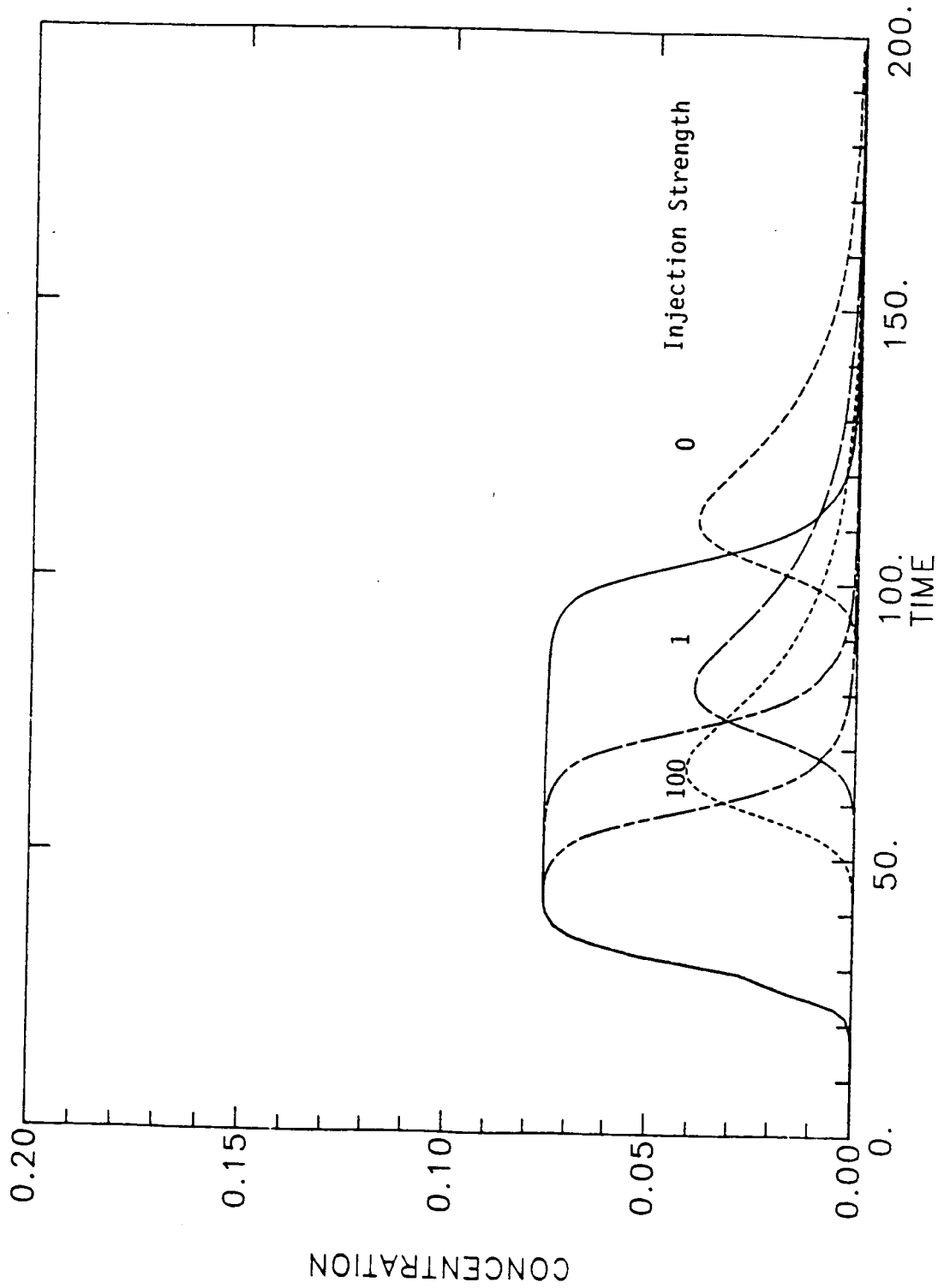
lasing we systematically varied the strength of the injection pulse. Figure 6 shows the system with W held at $.01 \text{ ns}^{-1}$ but varying the value of I from 0 to $I=1.0\text{e-}06 \text{ ns}^{-1}$ and $I=1.0\text{e-}04 \text{ ns}^{-1}$. Clearly, the presence of the injection beam speeds up the onset of stimulated emission. The RKF algorithm worked efficiently in these examples, with each case requiring no more than 846 derivative evaluations.

The theorem of the previous section demonstrates that this system of equations is asymptotically stable and the numerical calculations evidence this same stability for a wide range of values of the pump intensity. The non-linearity of the system will support relaxation oscillations at the onset of lasing before the stable state is reached. An illustration of these oscillations is shown in Fig. 7. The variations of the inversion and photon density are shown in separate graphs and also combined together in a phase portrait. An extensive study of the relaxation oscillations of this system will appear elsewhere [10].

SUMMARY AND CONCLUSION

We have developed a model of the dynamics of an end-pumped injection seeded, four level laser. The model was developed in order to examine the early transient behavior of tunable solid state lasers and the effects of injection seeding on the timing and shape of the output laser pulse. In this paper we report on our analysis of the quantitative behavior of solution to the model and on the quality of the numerical computation of these solutions.

we have demonstrated the existence of integrable solutions to the system of equations forming the model provided that the pump and injection source functions are sufficiently regular and that the initial conditions



RATE EQUATION MODEL

Figure 6. The effects of increasing the intensity of the injection signal is to initiate the laser pulse at earlier times and to narrow the pulse shape.

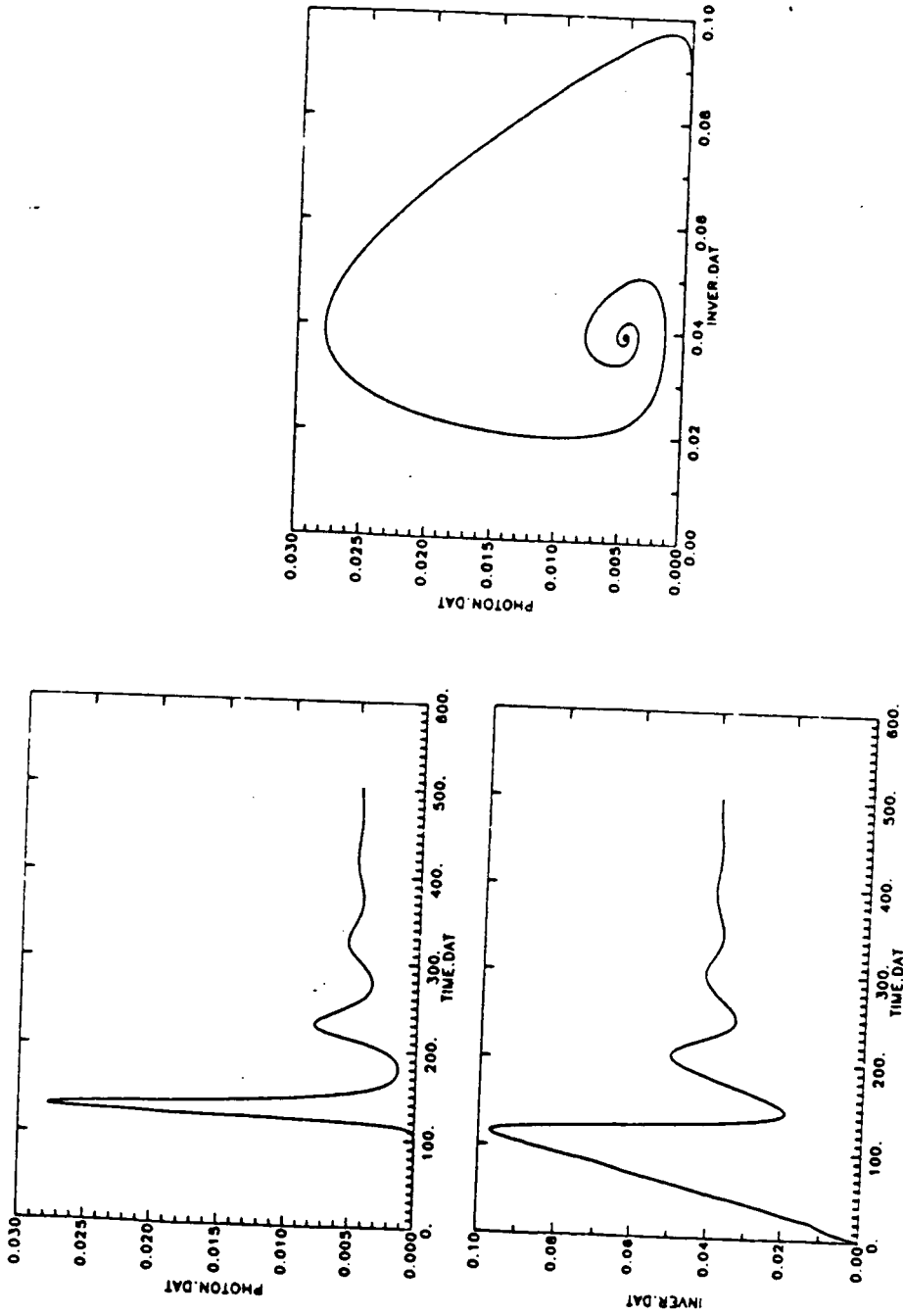


Figure 7. Inversion and photon densities illustrating relaxation oscillations before stable solution is reached. Individual curves are combined together in a phase portrait.

are physically realizable. Furthermore, we show that these solutions are asymptotically stable and establish bounds on them.

The equations were solved numerically and the sensitivity of the numerical calculations to input parameter values was studied. A general tendency toward stiffening of the system with increasing pump energy was noted. The validity of the model in the anticipated operating regime was established.

ADDENDUM

The material in this report is presently being prepared for submission to the journal, Mathematical Modeling. Co-authors are A. M. Buoncristiani and L. F. Roberts.

ACKNOWLEDGMENTS

This work was supported by NASA/Langley Research Grant NAG-1-704. The project was monitored by Dr. Charles E. Byvik, FED-Laser Technology and Applications Branch.

REFERENCES

1. Brockman, P., C. H. Blair, J. C. Barnes, R. V. Hess, and E. V. Browell. Optics Letters, Vol. 11, No. 11, pp. 712-714 (1986).
2. Y. K. Park, G. Gullani, and R. L. Byer, IEEE J. Quantum Electron, QE-20, 117 (1984).
3. Harter, D. J., J. J. Yeh, A. J. Heiney, and D. R. Siebert, Digest of Topical Meeting on Tunable Solid State Lasers (Optical Society of America, Washington, D.C., 1985), paper FA2.
4. Park, Y. K. and R. L. Byer, Opt. Commun. 37, 411 (1981).
5. Moulton, P., Jour. Opt. Soc. Am. B, Vol. 3, No. 1, pp. 125-133 (1986).
6. Byvik, C. E. and A. M. Buoncristiani, IEEE J. Quantum Electron, QE-21, 1619 (1985).

7. Braver, F. and J. A. Nohel, The Qualitative Theory of Ordinary Differential Equations, (W. A. Benjamin, Inc., New York, 1969).
8. Burden, Richard L. and J. Douglas Faires, Numerical Analysis, (Prindle, Weber, and Schmidt, Boston, 1985).
9. Langley Research Center implementation of LSODE, On ODE software package based on the GEAR and CEARB packages (A.C. Hindmarsh, Lawrence Livermore Laboratory).
10. A. M. Buoncristiani, L.F. Roberts and J. Swetits, Stability of 3- and 4-level Lasers systems, to appear as NASA Technical Note.